Research Article | Vol. 28, No. 15 / 20 July 2020 / Optics Express 22732
Optics EXPRESS

Modeling broadband cloaking using 3D nano-assembled plasmonic meta-structures

MD. IMRAN KHAN,[1] SAYANTANI GHOSH,[1] RYAN BAXTER,[2] AND ARNOLD D. KIM[3,*]

[1]Department of Physics, University of California, Merced, 5200 North Lake Road, Merced, CA 95343, USA
[2]Department of Chemistry and Chemical Biology, University of California, Merced, 5200 North Lake Road, Merced, CA 95343, USA
[3]Department of Applied Mathematics, University of California, Merced, 5200 North Lake Road, Merced, CA 95343, USA
*adkim@ucmerced.edu

Abstract: The concept of "cloaking" an object is a very attractive one, especially in the visible (VIS) and near infra-red (NIR) regions of the electromagnetic spectrum, as that would reduce the visibility of an object to the eye. One possible route to achieving this goal is by leveraging the plasmonic property of metallic nanoparticles (NPs). We model and simulate light in the VIS and NIR scattered by a core of a homogeneous medium, covered by plasmonic cloak that is a spherical shell composed of gold nanoparticles (AuNPs). To consider realistic, scalable, and robust plasmonic cloaks that are comparable, or larger, in size to the wavelength, we introduce a multiscale simulation platform. This model uses the multiple scattering theory of Foldy and Lax to model interactions of light with AuNPs combined with the method of fundamental solutions to model interactions with the core. Numerical results of our simulations for the scattering cross-sections of core-shell composite indicate significant scattering suppression of up to 50% over a substantial portion of the desired spectral range (400 - 600 nm) for cores as large as 900 nm in diameter by a suitable combination of AuNP sizes and filling fractions of AuNPs in the shell.

1. Introduction

Advances in nano-synthesis [1–3] and nano-assembly [4–8] have opened up possibilities of many intriguing applications that seek to leverage not just the unique size-dependent properties of single nanoparticles (NPs), but also the collective behavior of ensembles of NPs, which are distinct both from isolated NPs and from their bulk counterparts [9,10]. One of these is the fabrication of meta-materials using metallic NPs whose interaction with electromagnetic (EM) waves have demonstrated exotic and anomalous phenomena, including 'cloaking' [11–13]. The fundamental concept allowing for cloaking is the ability of metallic NPs to modify EM waves in the near- and far-field regimes, a characteristic known as plasmonics, which is tunable via NP size, shape, composition, and in an ensemble, inter-NP separation [14–22]. This property allows for achieving invisibility via scattering cancellation [23–29], a method of passive cloaking which requires no external power. The spectral band over which scattering is suppressed is controlled by the physical properties of the NPs that, in turn, control their plasmonic response. The cloaking technique is based on all angle scattering cancellation using a layer of plasmonic material with low or negative effective permittivity, and relies on producing a local polarization that is in "anti-phase" in reference to the target being cloaked. A well-designed cloaking cover may recover the near- and far-field incident wavefront, and is independent of the incident angle, form and polarization of the incident wave and location of the observer.

The most common type of structure that has experimentally demonstrated significant scattering suppression is a spherical core-shell construct [11,25,30], schematically represented in Fig. 1. The core is the target to be cloaked, and the shell consists of an amorphous arrangement of

#395840 https://doi.org/10.1364/OE.395840
Journal © 2020 Received 23 Apr 2020; revised 31 May 2020; accepted 3 Jun 2020; published 16 Jul 2020

Optics EXPRESS

metallic NPs, typically gold or silver. Even a single layer of NPs in the shell has reduced scattering significantly, although the spatial size of the cores cloaked is limited to the subwavelength scale, and the spectral band of operation is relatively narrow – on the order of tens of nanometers. Theoretical predictions [31–33] have outlined the possibility that multilayered plasmonic covers could extend both the physical scale of targets and the operation wavelength ranges over which they are cloaked. Such structures face both experimental and theoretical challenges, as they are difficult to fabricate and scale up using traditional top-down and bottom-up approaches, and additionally, complicated to simulate, given that the most prevalent approach for the latter is based on a dipole approximation.

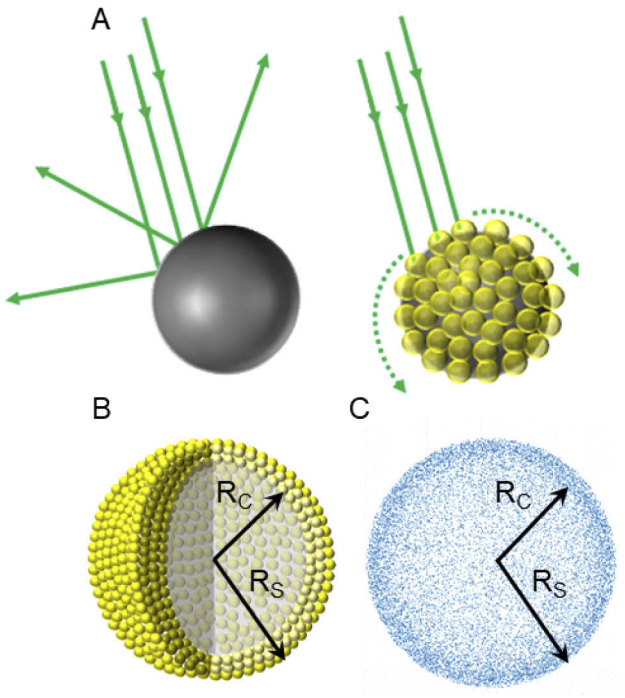

Fig. 1. Plasmonic cloaking with 3D nano-assembled shells. (a) Schematic depicting the difference of optical scattering from a bare sphere [left] and sphere coated with AuNPs [right] (b) Shell of finite-sized AuNPs of thickness $R_s - R_c$ surrounding the core of radius R_c (c) The corresponding set of point scatterers used in the model.

We have established a method [34,35] of nano-assembly capable of fabricating multi-layered plasmonic covers in the form of shells. These are 3D hollow constructs whose radii can be tuned from 200 nm – 2 μm and whose wall consists of several layers of densely packed AuNPs (see Fig. 1(b)). Effective medium theory [36] is not valid for modeling the multiple and densely packed AuNP layers forming these shells. Instead, a new multiscale modeling and simulation platform is needed to account for the strong multiple interactions of light with the individual AuNPs making up the shell. Additionally, this model must take into account interactions with the core. Because the strong, multiple interactions between the core and the AuNPs are the main mechanisms to be featured in this model, the power scattered and absorbed by the shell due to the optical properties of an individual AuNP need to be taken into account.

Here, we present a multiscale modeling and simulation platform that satisfies these requirements, and provides valuable insights into the relevant issues, such as the fact that scattering efficiency of a plasmonic cloak is suppressed most when each individual metal NP in the shell scatters and absorbs strongly. As strong multiple scattering in the shell assists with confining power to the

Optics EXPRESS

shell, it therefore follows that strong absorption in the shell attenuates the overall power scattered by the cloak. Results from our simulations are consistent with this interpretation.

In this model, scattering by the core is computed using the Method of Fundamental Solutions (MFS) [37] or Discrete Source Method [38]. Since the AuNPs are small compared to the wavelength, we model them as point scatterers (see Fig. 1(c)) and use the multiple scattering theory of Foldy [39] and Lax [40] to compute multiple scattering by them. We combine these two methods to obtain generalized Foldy-Lax [41] theory for this problem. Using this multiscale simulation platform, we compute the scattering efficiency of a plasmonic cloak for core diameters between 400 nm and 900 nm, gold NPs (AuNPs) with diameters of 5 nm, 10 nm, and 20 nm, and filling fraction of metal NPs in the shell between 0% and 65%. Through these simulations, we show that significant suppression of power is achieved for a broad spectral window from approximately 400 nm to 630 nm depending on the specific parameter values.

The remainder of this paper is as follows. We give a brief description of the method used to fabricate nano-assembled hollow shells composed of densely packed metal NPs in Section 2. In Section 3 we give the details of the multiscale model used to compute the scattering efficiency of a plasmonic cloak. Included in Section 3 is a detailed description of modeling assumptions and choices as well as validation studies. Results from using this model to compute the scattering efficiency for several different plasmonic cloaks is given in Section 4. We give our conclusions in Section 5. Appendix A gives the details of the model and Appendix B gives the method we use to compute the total scattering cross-section that is used for all the results shown here.

2. Design and fabrication

Shell formation is driven by a process reported in our earlier work [34,35]. This process leverages the phase transition of thermotropic hosts to assemble NPs dispersed in it into three-dimensional (3D) structures. The first step is to modify the surface of the NPs. The native ligands on the NPs are exchanged with custom-designed aromatic molecules, followed by dispersion of the NPs into a liquid crystal (LC) material. We use a commercially available LC, known as 5CB, as the host, and the functionalized NPs are added at 40° C when 5CB is in its isotropic (disordered) phase. This allows uniform dispersion, and is followed by decreasing the temperature of the suspension at the rate of 0.5° C/s down to 33° C. 5CB transitions from isotropic to nematic (ordered) phase at 35.5° C, so as the temperature decreases and the LC order parameter increases, it expels the previously well-dispersed NPs into shrinking isotropic domains. This proximity allows the ligands on the NPs to begin the shell formation through an attractive π-π interaction of their aromatic rings. Once shell formation is complete, the structures are very robust, and impervious to increased temperature. Further, they can be extracted from the host LC and re-dispersed into other optically homogeneous solvents.

By a judicious choice of ligands, shell diameters can be controllably tuned from 200 nm to 2 μm. In addition to this scalability, there are other advantages offered by this novel nano-assembly method. The first is versatility, where NPs of different compositions (including metallic, semi-conducting and magnetic) and of a wide range of sizes can be used to form the shells. Therefore, the use of different sizes of AuNPs to allow tuning the operational spectral band with relative ease. The second is the capability of encapsulation offered by this assembly process. An inclusion of choice can be added to the LC medium concurrently with the functionalized NPs, and as the NP-LC composite is cooled, the inclusions are trapped within the shells. Encapsulation of organic fluorescent dye, quantum dots and fluorescent bacteria have been successfully demonstrated [35], and this ability offers an additional degree of functionality not accessible to solid core-shell structures.

Optics EXPRESS

3. Model

We model the plasmonic cloak as a sphere composed of a uniform dielectric medium (core) surrounded by a random distribution of point scatterers (shell). The key parameters for the core include the diameter d and the relative refractive index m given as the ratio of the refractive index of the sphere divided by that of the surrounding medium. The key parameters for the shell include the number and positions of point scatterers and their individual optical properties. The number and positions of the point scatterers depend on the shell thickness and the filling fraction. We evaluate the cloaking properties of this structure by computing its scattering efficiency over wavelengths ranging from 400 nm to 700 nm.

The key parameters described above of this model are all elementary quantities. Consequently, this model has no inherent limitations on size or material properties. The key challenge is modeling the strong multiple scattering of light in this system. To simplify the modeling, we use the scalar approximation [42, Chapter 13]. Even though the scalar approximation does not account for all of the physical details in the system, it effectively accounts for the redistribution of power due to the multiple interactions between the core and the surrounding AuNPs, and therefore the overall behavior of the scattered light. For this reason, this scalar theory provides valuable insight into the problem while also keeping the discussion relatively simple.

3.1. Mathematical formulation

In what follows, we give a mathematical formulation for scattering by the system comprised of the dielectric spherical core, and the shell composed of randomly distributed metal NPs. This formulation follows closely with formulations of multiple scattering given by Ishimaru [43], for example.

Suppose that the origin of a coordinate system lies at the center of the dielectric sphere. We denote the interior domain by $D = \{|\mathbf{r}|<d/2\}$ and the exterior domain by $E = \{|\mathbf{r}|>d/2\}$. The spherical surface $B = \{|\mathbf{r}| = d/2\}$ is interface between the interior and exterior. The interior field ψ^{int} satisfies

$$\left(\nabla^2 + k_1^2\right)\psi^{\text{int}} = 0, \quad \text{in } D, \tag{1}$$

with k_1 denoting the wavenumber for the dielectric sphere. Let N denote the number of point scatterers in the shell. The exterior field, ψ^{ext} satisfies

$$\left(\nabla^2 + k_0^2\right)\psi^{\text{ext}} = -k_0^2 \sum_{n=1}^{N} V_n \psi^{\text{ext}}, \quad \text{in } E. \tag{2}$$

Here, k_0 is the wavenumber for the exterior and V_n corresponds to the scattering potential for the nth metal NP. We write ψ^{ext} as the sum $\psi^{\text{ext}} = \psi^{\text{inc}} + \psi^{s}$ with ψ^{inc} denoting the incident field, and ψ^{s} denoting the scattered field. We must supplement the equations above with conditions on B as well as radiation conditions. In particular, we prescribe that

$$\psi^{\text{int}} = \psi^{\text{inc}} + \psi^{\text{s}} \quad \text{on } B, \tag{3}$$

and

$$\partial_\nu \psi^{\text{int}} = \partial_\nu \psi^{\text{inc}} + \partial_\nu \psi^{\text{s}} \quad \text{on } B, \tag{4}$$

with ∂_ν denoting the derivative along the normal on B pointing into E. Additionally, we require that ψ^{s} satisfies the Sommerfeld radiation condition. Equations (1) and (2) along with interface conditions Eqs. (3) and (4), and the requirement that ψ^{s} satisfies the Sommerfeld radiation condition constitute a complete mathematical description of the problem.

To compute the fields interior and scattered by the core, we make use of the Method of Fundamental Solutions (MFS) which is also known as the Discrete Source Method. This method

Optics EXPRESS

was introduced by Mathon and Johnston [37]. It provides an accurate and efficient computational method for solving the full scattering problem [38]. Scattering by the metal NPs in the shell is computed using the self-consistent scattering theory due to Foldy [39] and Lax [40]. By combining these two theories, we arrive at the so-called generalized Foldy-Lax scattering theory introduced by Huang *et al.* [41] to study scattering by a system made up of an extended scatterer surrounded by smaller scatterers. This model contrasts with that by Huang *et al.* in that we use the MFS instead of a boundary integral equation method to model scattering by the extended object which is the core in our model. The details of this method are given in Appendix A. In Appendix B, we show how to compute the total scattering cross-section for the plasmonic cloak using the results from this method.

3.2. Modeling assumptions and choices

The key modeling assumption is that each metal NP is small enough that we can approximate it by a point scatterer. A point scatterer has a constant (complex) scattering amplitude, which we denote here by α. Scattering by a point scatterer is isotropic. Hence, its scattering cross-section σ_s is given by

$$\sigma_s = 4\pi|\alpha|^2. \tag{5}$$

Additionally, by the Optical Theorem or forward scattering theorem [42–45], we have

$$\sigma_t = \frac{4\pi}{k_0}\mathrm{Im}[\alpha]. \tag{6}$$

It follows that if σ_s and σ_t for an individual metal NP are known, then

$$\alpha = \left[\frac{\sigma_s}{4\pi} - \left(\frac{k_0\sigma_t}{4\pi}\right)^2\right]^{1/2} + \mathrm{i}\frac{k_0\sigma_t}{4\pi}. \tag{7}$$

In our model, we consider the metal NPs in the shell are identical in size and composition, so that there is only one scattering amplitude α needed for all N metal NPs. This assumption is not a restriction of the model. In fact, the details of the method described in Appendix A allow for a polydisperse distribution of metal NPs, each having different scattering amplitudes. Using a monodisperse distribution of metal NPs is a modeling choice based on the fabrication and design of these plasmonic cloaks described in Section 2. The ligands described in Section 2 may affect the optical properties of the shell and therefore would need to be included in the model. However, experimental measurements have not shown any significant scattering, extinction, or other optical signature from the ligands, over a range of 350 – 800 nm. Therefore, we neglect the ligands here and consider only scattering by the metal NPs as the main mechanism in this model leading to strong, multiple interactions between the core and shell.

In the results shown here, we have taken the optical properties for the metal NPs from experiments done on plasmonic film developed for plasmonic and nanophotonic applications. The measurements for gold are taken from Yakubovsky *et al.* [46], and the measurements for silver are taken from McPeak *et al.* [47]. The plasmonic films in those experiments were fabricated depositing polycrystalline grains whose diameter is approximately same as the film thickness. The plasmonic properties and grain diameter motivated us to use dielectric data from these sources. With those data, we compute the scattering cross-section σ_s and the total scattering cross-section σ_t used to define α in Eq. (7) using Rayleigh scattering theory [43–45].

Finally, these core-shell meta-structures depend on several parameters such as core diameter, NP diameter, shell thickness, volume filling fraction of the NP in the shell, etc. The model described in Appendix A can account for all of these system parameters. Nonetheless, we have chosen to focus here on the specific case in which the shell thickness is three times the constituent

Optics EXPRESS

metal NP diameter. This modeling choice is based on and consistent with the fabrication and design of the plasmonic cloaks described in Section 2. Moreover, it provides a useful restriction allowing for us to study individual system parameters such as the filling fraction, core diameter, and metal NP diameter in a controlled way.

3.3. Computational procedure

We give the computational procedure to compute the total scattering cross-section for a plasmonic cloak. This model requires specifying the relative refractive index m and diameter d of the core, and the diameter of an individual metal NPs. Once those values are specified, we perform the following computational procedure.

1. Compute the scattering and absorption cross-section for an individual metal NP using the experimentally measured optical properties for gold [46] or silver [47]. With those data, we compute the cross-sections for the metal NPs using Rayleigh scattering [43–45]. Those cross-sections are then used to compute α through evaluation of Eq. (7).

2. Specify the filling fraction f which gives the volume of all N metal NPs divided by the volume of the shell. Using that, we compute

$$N = \left\lfloor f \frac{\text{volume of shell}}{\text{volume of metal NP}} \right\rfloor, \tag{8}$$

   with $\lfloor x \rfloor$ denoting the floor function giving the largest integer that is less than or equal to x.

3. Compute the positions of the metal NPs, $\mathbf{r}_n^{\text{NP}}$ for $n = 1, \ldots, N$. For each metal NP, we compute three, pseudo-random numbers: r, θ, and φ. The radial length r is sampled uniformly over $R_c \leq r \leq R_s$ with $R_c = d/2$ and R_s denoting the outer radius of the shell set to be three times the diameter of one metal NP (see Section 3.1). The polar angle θ is uniformly sampled over $0 \leq \theta \leq \pi$, and the azimuthal angle φ is uniformly sampled over $0 \leq \varphi \leq 2\pi$. The coordinates for the center of a metal NP are $x = r\sin\theta\cos\varphi$, $y = r\sin\theta\sin\varphi$, and $z = r\cos\theta$. The algorithm checks positions of subsequent NPs for overlap and vacancy with other metal NPs. If the algorithm detects an overlap, that computed coordinate is discarded and another coordinate is computed. This process of generating non-overlapping coordinates is continued until it finishes generating N positions.

4. Use the Fibonacci lattice [48] to compute boundary points $\mathbf{r}_j \in B$ for $j = 1, \ldots, M$ and compute $\mathbf{r}_j^{\text{int}}$ and $\mathbf{r}_j^{\text{ext}}$ using Eqs. (A2) and (A6), respectively. In our simulations, we have set $M = 512$ and $\ell = 0.125d$.

5. Solve the linear system comprised of Eqs. (A11)–(A13) with $\psi^{\text{inc}}(\mathbf{r}) = e^{ik_0\hat{\mathbf{z}}\cdot\mathbf{r}}$ to determine the expansion coefficients, c_j^{int} and c_j^{ext} for $j = 1, \ldots, M$, and exciting fields, $\Psi_E(\mathbf{r}_n^{\text{NP}})$ for $n = 1, \ldots, N$

6. Evaluate Eq. (B5) at $\hat{\mathbf{i}} = \hat{\mathbf{o}} = \hat{\mathbf{z}}$ and use that to compute the total scattering-cross section according to Eq. (B6).

Steps 5 and 6 are repeated for each wavelength sampling the spectrum.

There are two parts of this procedure that require the most computational effort. Step 3 for computing the positions of the N metal NPs requires large computational times as N increases because each additional metal NP requires checking for overlap with the previous metal NPs. Future modifications to the computational platform will seek more efficient methods for determining these positions. The other major computational effort is Step 5 which requires solution of the $2MN \times 2MN$ linear system of equations. The corresponding system matrix is

Optics EXPRESS

dense and full. In the results shown here, we have only used a general Gaussian elimination method to solve this linear system. Therefore, this computation has a complexity of $O(8M^3N^3)$. However, the entries of the system matrix are mostly evaluations of Green's functions which yield an inherent structure in the system matrix that may be exploited for more efficient computations. Future modifications to the computational platform will seek to use state-of-the-art numerical linear algebra methods to make this computation more efficient.

3.4. Validation

Before proceeding to simulate the scattering efficiency and suppression of the nano-assembled shell structures, it is important to validate the model. We do so by first studying the accuracy of the MFS in computing scattering by the dielectric core without the shell of metal NPs to demonstrate the high accuracy achieved with this method. For a second validation study, we apply our model to the system studied by Mühlig *et al.* [11], where silver NPs (AuNPs) are used to decorate the surfaces of silica cores to show that the model captures features that are not predicted using Maxwell-Garnett theory.

Consider the plane wave $\psi^{\text{inc}} = e^{ik_0\mathbf{r}\cdot\hat{\mathbf{z}}}$ incident on a silica sphere with relative refractive index $m = 1.4$ and diameter $d = 750$ nm. For this problem, we can determine the solution of this scattering problem exactly. The scattered field is given as an expansion in Legendre polynomials whose expansion coefficients can be determined analytically. To compute the scattered field using the MFS, we use the method described in Appendix A, but without terms corresponding to scattering by the metal NPs so that $\Psi_n = 0$, identically. This leads to a $2M \times 2M$ linear system corresponding to Eqs. (A11) and (A12) with $\alpha_n = 0$. The code used to compute these results along with extensive documentation is available at the GitHub repository [49].

In the left plot of Fig. 2 we show the scattering efficiency σ_E defined as the total scattering cross-section σ_t normalized by the geometric cross-section, $\sigma_g = \pi d^2/4$. The solid blue curve is the result from the first 64 terms of the Legendre expansion for the exact solution and the orange circles is the result from the MFS approximation. These results show excellent agreement. In the right plot of Fig. 2 we show the relative error made by the MFS approximation. Over the spectral window, we find that the MFS is highly accurate with relative errors less than 0.1%. We have found that the MFS performs consistently well for a broad range of sphere diameters thereby demonstrating its effectiveness in modeling scattering by the core.

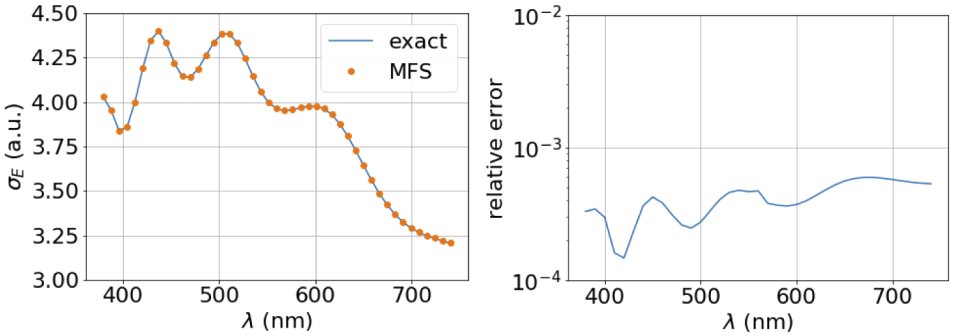

Fig. 2. Comparison of the exact solution and the MFS approximation for a silica sphere with relative refractive index $m = 1.4$ and diameter $d = 750$ nm. The left plot shows the scattering efficiency σ_E given by the total scattering cross-section σ_t normalized by the geometric cross-section $\sigma_g = \pi d^2/4$. The solid blue curve is the result from the exact solution and the orange circles is the result computed using the MFS. The right plot shows the relative error of the MFS approximation.

Optics EXPRESS

For the full model that includes many metal NPs in a shell surrounding the dielectric core, there is no analytical solution available. Instead, we have applied this model to plasmonic cloaks studied experimentally by Mühlig *et al.* [11]. For this comparison, we have used a relative refractive index of $m = 2.18$ and diameter $d = 55$ nm for the silica core. We have used a filling fraction of $f = 10\%$ for the AgNPs on the surface of the core. This comparison was done using only one realization of the AgNPs positions, so no averaging was done to compute the simulation results. No other tuning of our model was done in this comparison study.

Figure 3 shows the data from the experiment by Mühlig *et al.* [11] (solid squares), where a scattering suppression is observed between 340 – 390 nm, as is expected, given the spectral band of the plasmonic resonance of silver. The calculated values derived from Maxwell-Garnett theory reported by Mühlig *et al.* [11] are also plotted (triangles). According to Maxwell-Garnett theory, the maximum suppression range is 300 – 350 nm, which is blue-shifted from the experimental data. In contrast, the results of our simulation (circles) are in closer agreement to the experimental results.

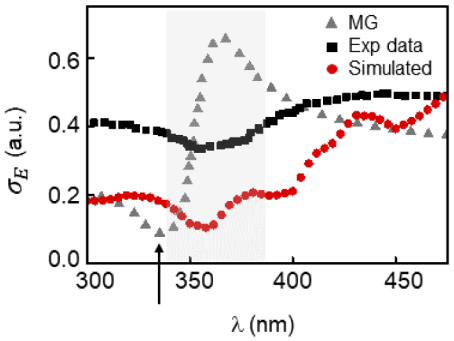

Fig. 3. Experimental results (Exp data) by Mühlig *et al.* [11] for the scattering efficiency σ_E compared with Maxwell-Garnett theory (MG) and results from our model (simulated). The gray-shaded region highlights the agreement between the experimental results and our model. The arrow indicates the scattering minimum predicted by Maxwell-Garnett theory which, is blue-shifted from the other two results.

The results shown in Fig. 3 demonstrate the usefulness of this new model. It compliments the Maxwell-Garnett approximation by providing a different interpretation for scattering suppression. The fundamental mechanisms in this model is the multiple interactions included between the metal NPs and the dielectric core. Most importantly, it has the capability of scaling up to larger systems without restriction. In what follows, we use this model to study the scattering suppression properties of plasmonic cloaks.

4. Results and discussion

In the simulation results that follow, we consider a core made of silica with relative refractive index assumed to be $m = 1.4$ over the spectral window of 400 nm to 700 nm, and AuNPs with diameters of 5 nm, 10 nm, and 20 nm. The shell thickness is set to be three times the diameter of an individual AuNP and the ligand length is assumed to be 0.98 nm. We show results for different values of the core diameter d and filling fractions f. In particular, we plot the scattering efficiency, σ_E, defined according to

$$\sigma_E = \sigma_t(\lambda)/\sigma_g, \tag{9}$$

with σ_g denoting the geometric cross-section. For reference, we compare our results for the scattering efficiency of plasmonic cloak with that for the silica core alone. The geometric

Optics EXPRESS

cross-section for the silica core is $\sigma_g = \pi R_c^2$ with $R_c = d/2$ denoting the core radius, and the geometric cross-section for the plasmonic cloak is $\sigma_g = \pi R_s^2$ with R_s denoting the shell outer radius.

Figure 4 summarizes our results for a $d = 750$ nm silica core covered with plasmonic cloak comprising 10 nm AuNPs of varying filling fraction f. The scattering efficiency for the bare silica core, σ_E^C, shows the characteristic oscillatory behavior seen in Mie theory [44,45]. The peaks of those oscillations correspond to so-called Mie resonances. The locations and heights of those peaks are characteristic of the size and relative refractive index of the sphere. The scattering efficiency for the core with the plasmonic shell (σ_E^{CS}) composed of 10 nm AuNPs for all $f = 0.05, f = 0.10$, and $f = 0.30$ shown in Figs. 4(a)–4(c) demonstrate a suppression in the spectral range 400 – 550 nm where the core -shell composite shows little to no trace of the Mie resonances associated with the silica core. Thus, the spectral signature of the core is effectively removed by the shell of AuNPs. As intuitively expected, the scattering suppression $\Delta\sigma_E$ (defined as $\sigma_E^C - \sigma_E^{CS}$), increases with the filling fraction f.

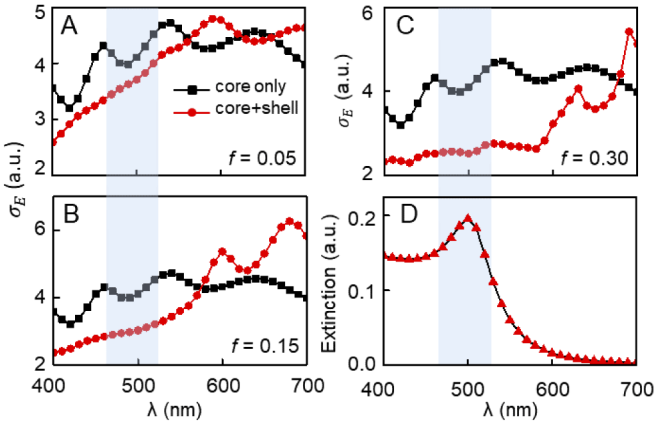

Fig. 4. Comparisons of the scattering efficiency σ_E for a 750 nm silica core (square symbols) with that for a core and shell (circle symbols) made up of 10 nm AuNPs for filling fractions (a) $f = 0.05$, (b) $f = 0.15$, and (c) $f = 0.30$. The extinction spectrum for a single 10 nm AuNP is shown in (d), with its FWHM band highlighted in blue in (a) - (d).

This spectral region over which the plasmonic shell cover suppresses the scattering of the core occurs corresponds closely to the FWHM spectral band of the extinction spectrum of a single AuNP (Fig. 4(d) highlighted in blue) highlighting that the main mechanism in this model is the multiple scattering due to the AuNPs and the dielectric core. Consequently, scattering suppression of the plasmonic cloak depends strongly on scattering and absorption by each individual AuNP. When scattering by an individual metal NP is strong, power incident on the shell of AuNPs undergoes strong multiple scattering in the shell. When absorption by each AuNP is also strong, this strong multiple scattering effectively yields higher absorption of the overall power. Thus, strong scattering creates multiple interactions with strong absorbing AuNPs thereby yielding a suppression in power scattered by the plasmonic cloak.

Figure 5 shows results that compare plasmonic cloaks with 5 nm and 20 nm AuNPs for the same 750 nm diameter silica core. Recall that the shell thickness is set to be three times the diameter of the AuNP. Thus, for the 5 nm diameter AuNP, the shell thickness is 15 nm and for 20 nm diameter AuNPs, the shell thickness is 60 nm. It then follows that the filling fraction sets the corresponding number of AuNPs contained in the shell.

In Fig. 5 the black curves with square symbols show the scattering efficiency for the silica core, the green curves with triangle symbols show the scattering efficiency for the plasmonic

Optics EXPRESS

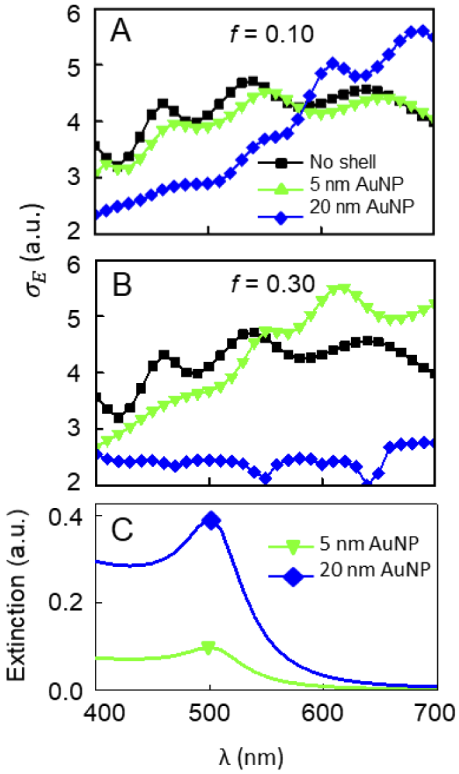

Fig. 5. Comparisons of the scattering efficiency σ_E for a 750 nm silica core (square symbols) with that by a core and shell made up of 5 nm AuNPs (triangle symbols) and 20 nm AuNPs (diamond symbols) for filling fractions (a) $f = 0.10$, and (b) $f = 0.30$. A comparison of the extinction for single 5 and 20 nm AuNP is shown in (c).

cloak made up of 5 nm diameter AuNPs, and the blue curves with diamond symbols show the scattering efficiency for the plasmonic cloak made up of 20 nm diameter AuNPs. Figure 5(a) is for filling fraction $f = 0.10$ and Fig. 5(b) is for filling fraction $f = 0.30$. Figure 5(c) shows the extinction for an individual 5 nm diameter (green curve) and 20 nm diameter AuNP (blue curve).

Because Fig. 5(c) shows that the extinction for the 20 nm diameter AuNP is relatively larger than that for the 5 nm diameter AuNP, we expect that the scattering suppression by the plasmonic cloak made up of 20 nm diameter AuNPs to be greater than that for a plasmonic cloak made up of 5 nm diameter AuNPs. The results in Figs. 5(a) and (b) show this to be the case. We observe substantially more suppression of scattering using the 20 nm diameter AuNPs in comparison with the 5 nm AuNPs for both $f = 0.10$ and $f = 0.30$. For the larger filling fraction, we find that the 20 nm diameter AuNPs suppress scattering across the entire spectral range.

The results in Figs. 4 and 5 indicate that the plasmonic cloaks effectively suppress scattering over a broad spectral range. The amount of scattering suppression depends strongly on the filling fraction. To study the dependence on the filling fraction, we show in Fig. 6 a map of the scattering suppression $\Delta\sigma_E$. Here, the plasmonic cloak is made up of 10 nm AuNPs. Thus, when $\Delta\sigma_E>0$, it implies that incorporating the plasmonic shell cover reduces scattering from the core, and that cloaking is successful. And when $\Delta\sigma_E<0$, it signifies that scattering efficiency of the bare silica core is higher than the silica core-shell composite. The dark regions of Fig. 6 show where the plasmonic cloak is effective in suppressing scattering. These results show that both the magnitude of $\Delta\sigma_E$ and its operational spectral band are enhanced as the filling fraction increases.

Optics EXPRESS

Indeed, we observe that the onset of cloaking begins around a small value of $f \geq 25\%$ and rapidly improves thereafter.

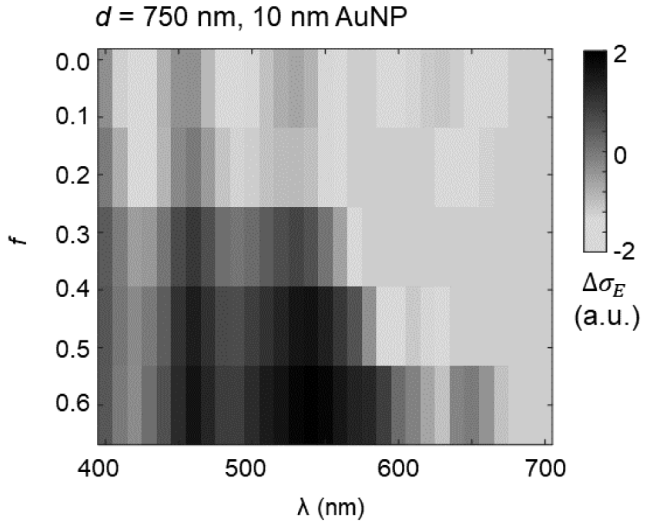

Fig. 6. A plot of the scattering suppression (scattering efficiency of silica core minus scattering efficiency of plasmonic cloak) as a function of filling fraction f and wavelength λ for a core diameter of 750 nm and AuNPs with diameter 10 nm.

Figure 7 maps $\Delta\sigma_E$ for different core diameters ranging from 400 nm to 900 nm. For these results, the plasmonic cloak is made up of 10 nm AuNPs and the filling fraction was held fixed at $f = 0.30$. For all of the silica core diameters shown here, we observe significant scattering suppression. An important point to note is that the ratio of the radius of AuNPs to the shell thickness is the same for all cases. This implies that, as the cores get larger, the ratio of shell wall to core-shell diameter decreases. This agrees with our experimental platform. Further, $\Delta\sigma_E>0$ for the entire range of core sizes leads to the conclusions that not only does a plasmonic shell

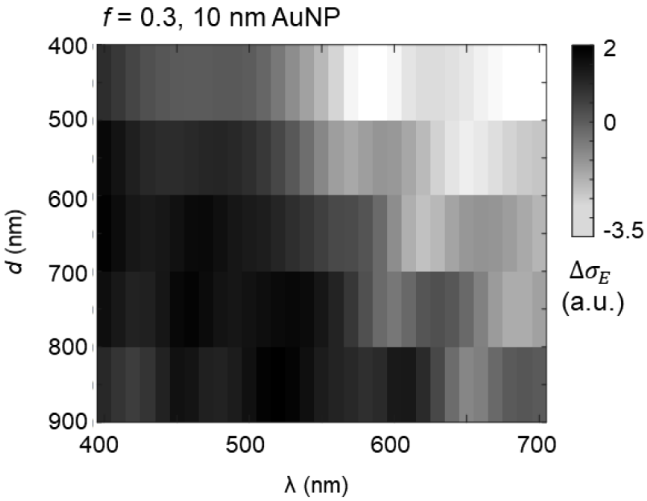

Fig. 7. A plot of the scattering suppression as a function of core diameter d and wavelength λ for a filling fraction of $f = 30\%$ and AuNPs with diameter 10 nm.

Optics EXPRESS

successfully cloak cores with $d \sim \lambda$, but in addition, do so without requiring the need to add more AuNP layers.

5. Conclusions

We have developed a computational platform to study plasmonic cloaking structures composed of a core surrounded by a shell of AuNPs. This model uses fundamental quantities such as the scattering and absorption cross-sections of the AuNPs and the material properties of the core by combining the Method of Fundamental Solutions to compute scattering by the core with Foldy-Lax theory to compute multiple scattering by the AuNPs. It also takes into account strong multiple interactions between the core and the AuNPs, which is essential for understanding complex plasmonic cloaks composed of multiple layers of NP coverings. And while it is limited because it uses the scalar approximation and a point scatterer assumption for the AuNPs, it nonetheless provides a useful tool for studying broadband 3D plasmonic cloaking.

Simulations results presented confirm that plasmonic NPs can be used to design cloaks in the visible part of the EM spectrum, and along with suppressing scattering over a broad spectral range, AuNPs robustly cloak silica cores as large as 900 nm, larger than the wavelength of operation. Additionally, as the core size increases, cloaking is successful without a subsequent increase in the layers of AuNPs, as shown by the suppression via a constant filling fraction.

Appendix A: computational model

We use the MFS to compute the interior field inside the core, ψ^{int}. In the whole space composed of a uniform medium with wavenumber k_1, Green's function,

$$G_1(\mathbf{r}-\mathbf{r}') = \frac{e^{ik_1|\mathbf{r}-\mathbf{r}'|}}{4\pi|\mathbf{r}-\mathbf{r}'|}, \tag{A1}$$

gives a spherical wave centered at $\mathbf{r}'$. We use the Fibonacci lattice [48] to compute boundary points $\mathbf{r}_j \in B$ for $j = 1, \ldots, M$ which are approximately uniformly distributed on the surface of the sphere. Then, we set

$$\mathbf{r}_j^{\text{int}} = \mathbf{r}_j + \ell\hat{\boldsymbol{\nu}}_j, \quad j = 1, \ldots, M, \tag{A2}$$

with $\hat{\boldsymbol{\nu}}_j$ denoting the unit outward normal at $\mathbf{r}_j$, and $\ell>0$ denoting a user-defined length parameter. In our simulations, we have set $\ell = 0.125d$. According to Eq. (A2), $\mathbf{r}_j^{\text{int}}$ for $j = 1, \ldots, M$ lie *outside* of the sphere. Using these points, we form the following approximation,

$$\psi^{\text{int}}(\mathbf{r}) \approx \sum_{j=1}^{M} c_j^{\text{int}} G_1(\mathbf{r}-\mathbf{r}_j^{\text{int}}), \quad \mathbf{r} \in D. \tag{A3}$$

Equation (A3) approximates ψ^{int} as a superposition of finitely many spherical waves centered at points located outside of D. Therefore, it is exactly satisfies Eq. (1).

We compute the exterior field, ψ^{ext} using the sum,

$$\psi^{\text{ext}} = \psi^{\text{inc}} + \psi^{B} + \sum_{n=1}^{N} \Psi_n, \tag{A4}$$

with ψ^B denoting the field scattered by the dielectric sphere and Ψ_n denoting the field scattered by the nth metal nanoparticle. Green's function,

$$G_0(\mathbf{r}-\mathbf{r}') = \frac{e^{ik_0|\mathbf{r}-\mathbf{r}'|}}{4\pi|\mathbf{r}-\mathbf{r}'|}, \tag{A5}$$

Optics EXPRESS

gives a spherical wave centered at $\mathbf{r}'$ propagating in the whole space with wavenumber k_0. Just as we have done in Eq. (A2), we set

$$\mathbf{r}_j^{\text{ext}} = \mathbf{r}_j - \ell\hat{\mathbf{v}}_j, \quad j = 1, \ldots, M. \tag{A6}$$

It follows that $\mathbf{r}_j^{\text{ext}}$ for $j = 1, \ldots, M$ lie *inside* the sphere. Consequently, the approximation given by

$$\psi^B(\mathbf{r}) \approx \sum_{j=1}^{M} c_j^{\text{ext}} G_0(\mathbf{r} - \mathbf{r}_j^{\text{ext}}) \tag{A7}$$

exactly satisfies

$$\left(\nabla^2 + k_0^2\right)\psi^B = 0, \quad \mathbf{r} \in E. \tag{A8}$$

Let $\mathbf{r}_n^{\text{NP}}$ denote the center of the nth AuNP whose scattering amplitude is α_n. The field scattered by the nth AuNP is then given by

$$\Psi_n = \alpha_n G_0(\mathbf{r} - \mathbf{r}_n^{\text{NP}})\Psi_E(\mathbf{r}_n^{\text{NP}}), \tag{A9}$$

with $\Psi_E(\mathbf{r}_n^{\text{NP}})$ denoting the exciting field at $\mathbf{r}_n^{\text{NP}}$. This exciting field is given as the sum,

$$\Psi_E(\mathbf{r}_n^{\text{NP}}) = \psi^{\text{inc}}(\mathbf{r}_n^{\text{NP}}) + \psi^B(\mathbf{r}_n^{\text{NP}}) + \sum_{\substack{n'=1 \\ n'\neq n}}^{N} \alpha_{n'} G_0(\mathbf{r}_n^{\text{NP}} - \mathbf{r}_{n'}^{\text{NP}})\Psi_E(\mathbf{r}_{n'}^{\text{NP}}). \tag{A10}$$

Equation (A10) gives the exciting field at $\mathbf{r}_n^{\text{NP}}$ as the sum of the incident field ψ^{inc}, the field scattered by the dielectric sphere ψ^B, and the fields scattered by all of the other $N-1$ metal nanoparticles evaluated at $\mathbf{r}_n^{\text{NP}}$.

In the expressions for ψ^{int}, ψ^B, and Ψ_n given by Eqs. (A3), (A7), and (A9), respectively, the quantities c_j^{int} for $j = 1, \ldots, M$, c_j^{ext} for $j = 1, \ldots, M$, and $\Psi_E(r_n)$ for $n = 1, \ldots, N$ are to be determined. We find them using interface conditions Eqs. (3) and (4). By requiring that interface condition Eq. (3) is satisfied exactly on the M boundary points, $\mathbf{r}_i \in B$ for $i = 1, \ldots, M$, we find that

$$\sum_{j=0}^{M} c_j^{\text{int}} G_1(\mathbf{r}_i - \mathbf{r}_j^{\text{int}}) - \sum_{j=1}^{M} c_j^{\text{ext}} G_0(\mathbf{r}_i - \mathbf{r}_j^{\text{ext}}) - \sum_{n=1}^{N} \alpha_n G_0(\mathbf{r}_i - \mathbf{r}_n^{\text{NP}})\Psi_E(\mathbf{r}_n^{\text{NP}}) = \psi^{\text{inc}}(\mathbf{r}_i), \quad i = 1, \cdots, M. \tag{A11}$$

Similarly, by requiring that boundary condition Eq. (4) is satisfied exactly on the M boundary points, we find that

$$\sum_{j=0}^{M} c_j^{\text{int}} \partial_\nu G_1(\mathbf{r}_i - \mathbf{r}_j^{\text{int}}) - \sum_{j=1}^{M} c_j^{\text{ext}} \partial_\nu G_0(\mathbf{r}_i - \mathbf{r}_j^{\text{ext}}) - \sum_{n=1}^{N} \alpha_n \partial_\nu G_0(\mathbf{r}_i - \mathbf{r}_n^{\text{NP}})\Psi_E(\mathbf{r}_n^{\text{NP}}) = \partial_\nu \psi^{\text{inc}}(\mathbf{r}_i), \quad i = 1, \cdots, M. \tag{A12}$$

Finally, by substituting Eq. (A7) into Eq. (A10) and rearranging terms, we find that

$$\Psi_E(\mathbf{r}_n^{\text{NP}}) - \sum_{\substack{n'=1 \\ n'\neq n}}^{N} \alpha_{n'} G_0(\mathbf{r}_n^{\text{NP}} - \mathbf{r}_{n'}^{\text{NP}})\Psi_E(\mathbf{r}_{n'}^{\text{NP}}) - \sum_{j=1}^{M} c_j^{\text{ext}} G_0(\mathbf{r}_n^{\text{NP}} - \mathbf{r}_j^{\text{ext}}) = \psi^{\text{inc}}(\mathbf{r}_n), \quad n = 1, \cdots, N. \tag{A13}$$

Equations (A11), (A12), and (A13) give $2MN$ equations for the $2MN$ unknowns: c_j^{int} for $j = 1, \ldots, M$, c_j^{ext} for $j = 1, \ldots, M$, and $\Psi_E(\mathbf{r}_n^{\text{NP}})$ for $n = 1, \ldots, N$. These equations can be combined to form a $2MN \times 2MN$ linear system that is solved using standard numerical linear algebra methods.

Optics EXPRESS

Appendix B: computing the total scattering cross-section

Upon solution of the linear system comprised of Eqs. (A11)–(A13) given above, the scattered field is given by

$$\psi^{\mathrm{s}}(\mathbf{r}) = \psi^{B} + \sum_{n=1}^{N} \Psi_n \approx \sum_{j=1}^{M} c_j^{\mathrm{ext}} G_0(\mathbf{r} - \mathbf{r}_j^{\mathrm{ext}}) + \sum_{n=1}^{N} \alpha_n G_0(\mathbf{r} - \mathbf{r}_n^{\mathrm{NP}}) \Psi_E(\mathbf{r}_n^{\mathrm{NP}}), \quad r \in E. \tag{B1}$$

The scattered field evaluated at $\mathbf{r} = R\hat{\mathbf{o}}$ with $R = |\mathbf{r}|$ and $\hat{\mathbf{o}} = \mathbf{r}/|\mathbf{r}|$ in the far-field corresponding to $R \gg 1$ behaves like a spherical wave and is given by [42–45]

$$\psi^{\mathrm{s}}(\mathbf{r}) \sim f(\hat{\mathbf{o}}, \hat{\boldsymbol{\imath}}) \frac{e^{\mathrm{i}k_0 R}}{R}. \tag{B2}$$

Here, $f(\hat{\mathbf{o}}, \hat{\boldsymbol{\imath}})$ is the scattering amplitude for the scattered field in the far field in direction $\hat{\mathbf{o}}$ when the particle is illuminated by a plane wave propagating in direction $\hat{\boldsymbol{\imath}}$ with unit amplitude.

Suppose we have set ψ^{inc} to be a plane wave of unit amplitude propagating in direction $\hat{\boldsymbol{\imath}}$ and we have used that to compute the solution of Eqs. (A11)–(A13). Using $|R\hat{\mathbf{o}} - \mathbf{r}'| \sim R - \hat{\mathbf{o}} \cdot \mathbf{r}'$ for $R \gg 1$, the far-field Green's function [42–45] is

$$G_0(R\hat{\mathbf{o}} - \mathbf{r}') \sim e^{\mathrm{i}k_0 \hat{\mathbf{o}} \cdot \mathbf{r}'} \frac{e^{\mathrm{i}k_0 R}}{4\pi R}, \quad R \gg 1. \tag{B3}$$

Replacing G_0 by Eq. (B3) in Eq. (B1) yields

$$\psi^{\mathrm{s}}(\mathbf{r}) \sim \left[\frac{1}{4\pi} \sum_{j=1}^{M} c_j^{\mathrm{ext}} e^{\mathrm{i}k_0 \hat{\mathbf{o}} \cdot \mathbf{r}_j^{\mathrm{ext}}} + \sum_{n=1}^{N} \alpha_n e^{\mathrm{i}k_0 \hat{\mathbf{o}} \cdot \mathbf{r}_n^{\mathrm{NP}}} \Psi_E(\mathbf{r}_n^{\mathrm{NP}}) \right] \frac{e^{\mathrm{i}k_0 R}}{R}, \quad R \gg 1. \tag{B4}$$

By comparing Eq. (B2) with Eq. (B4), we find that the scattering amplitude using our method is given by

$$f(\hat{\mathbf{o}}, \hat{\boldsymbol{\imath}}) \approx \frac{1}{4\pi} \sum_{j=1}^{M} c_j^{\mathrm{ext}} e^{\mathrm{i}k_0 \hat{\mathbf{o}} \cdot \mathbf{r}_j^{\mathrm{ext}}} + \frac{1}{4\pi} \sum_{n=1}^{N} \alpha_n e^{\mathrm{i}k_0 \hat{\mathbf{o}} \cdot \mathbf{r}_n^{\mathrm{NP}}} \Psi_E(\mathbf{r}_n^{\mathrm{NP}}). \tag{B5}$$

According to the Optical Theorem or forward scattering theorem [42–45], we can compute the total cross-section σ_t of the scattering structure through evaluation of

$$\sigma_t = \frac{4\pi}{k_0} \mathrm{Im}[f(\hat{\boldsymbol{\imath}}, \hat{\boldsymbol{\imath}})]. \tag{B6}$$

We compute the total cross-section by substituting Eq. (B5) into this formula. Remarkably, Eq. (B6) allows for the determination of σ_t by only measuring the power scattered in the forward direction.

Funding

National Science Foundation (CHE-1752821, DMS-1819052, DMS-1840265, HRD-1547848); Air Force Office of Scientific Research (FA9550-17-1-0238, FA9550-18-1-0519).

Disclosures

The authors declare no conflicts of interest.

Optics EXPRESS

References

1. K. Yao and Y. Liu, "Plasmonic metamaterials," Nanotechnol. Rev. **3**(2), 177–210 (2014).
2. G. V. Eleftheriades and K. G. Balmain, *Negative-Refraction Metamaterials* (Wiley, New York, 2005).
3. N. Engheta and R. W. Ziolkowski, *Metamaterials: Physics and Engineering Explorations* (Wiley, New York, 2006).
4. W. Zhao and X. Zhao, "Fabrication and characterization of metamaterials at optical frequencies," Opt. Mater. **32**(3), 422–426 (2010).
5. L. O. Herrmann, V. K. Valev, C. Tserkezis, J. S. Barnard, S. Kasera, O. A. Scherman, J. Aizpurua, and J. J. Baumberg, "Threading plasmonic nanoparticle strings with light," Nat. Commun. **5**(1), 4568 (2014).
6. M. I. Stockman, "Nanoplasmonics: past, present, and glimpse into future," Opt. Express **19**(22), 22029–22106 (2011).
7. M. Jablan, H. Buljan, and M. Soljačić, "Plasmonics in graphene at infrared frequencies," Phys. Rev. B **80**(24), 245435 (2009).
8. P. Dey, S. Zhu, K. J. Thurecht, P. M. Fredericks, and I. Blakey, "Self assembly of plasmonic core-satellite nano-assemblies mediated by hyperbranched polymer linkers," J. Mater. Chem. B **2**(19), 2827–2837 (2014).
9. H. Chen, "Metamaterials: Constitutive parameters, performance, and chemical methods for realization," J. Mater. Chem. **21**(18), 6452–6463 (2011).
10. P. R. West, S. Ishii, G. V. Naik, N. K. Emani, V. M. Shalaev, and A. Boltasseva, "Searching for better plasmonic materials," Laser Photonics Rev. **4**(6), 795–808 (2010).
11. S. Mühlig, A. Cunningham, J. Dintinger, M. Farhat, S. B. Hasan, T. Scharf, T. Bürgi, F. Lederer, and C. Rockstuhl, "A self-assembled three-dimensional cloak in the visible," Sci. Rep. **3**(1), 2328 (2013).
12. R. Fleury, F. Monticone, and A. Alù, "Invisibility and cloaking: Origins, present, and future perspectives," Phys. Rev. Appl. **4**(3), 037001 (2015).
13. B. Edwards, A. Alù, M. G. Silveirinha, and N. Engheta, "Experimental verification of plasmonic cloaking at microwave frequencies with metamaterials," Phys. Rev. Lett. **103**(15), 153901 (2009).
14. A. Alù and N. Engheta, "Cloaking and transparency for collections of particles with metamaterial and plasmonic covers," Opt. Express **15**(12), 7578 (2007).
15. D. S. Filonov, A. P. Slobozhanyuk, P. A. Belov, and Y. S. Kivshar, "Double-shell metamaterial coatings for plasmonic cloaking," Phys. Status Solidi RRL **6**(1), 46–48 (2012).
16. C. Argyropoulos, P. Y. Chen, F. Monticone, G. D'Aguanno, and A. Alù, "Nonlinear plasmonic cloaks to realize giant all-optical scattering switching," Phys. Rev. Lett. **108**(26), 263905 (2012).
17. A. Alù and N. Engheta, "Effects of size and frequency dispersion in plasmonic cloaking," Phys. Rev. E **78**(4), 045602 (2008).
18. S. Tricarico, F. Bilotti, A. Alù, and L. Vegni, "Plasmonic cloaking for irregular objects with anisotropic scattering properties," Phys. Rev. E **81**(2), 026602 (2010).
19. S. Mühlig, M. Farhat, C. Rockstuhl, and F. Lederer, "Cloaking dielectric spherical objects by a shell of metallic nanoparticles," Phys. Rev. B **83**(19), 195116 (2011).
20. S. Mühlig, A. Cunningham, J. Dintinger, T. Scharf, T. Bürgi, F. Lederer, and C. Rockstuhl, "Self-assembled plasmonic metamaterials," Nanophotonics **2**(3), 211–240 (2013).
21. M. Farhat, P. Y. Chen, S. Guenneau, S. Enoch, R. McPhedran, C. Rockstuhl, and F. Lederer, "Understanding the functionality of an array of invisibility cloaks," Phys. Rev. B **84**(23), 235105 (2011).
22. A. Monti, F. Bilotti, and A. Toscano, "Optical cloaking of cylindrical objects by using covers made of core-shell nanoparticles," Opt. Lett. **36**(23), 4479 (2011).
23. P. Y. Chen, J. Soric, and A. Alù, "Invisibility and cloaking based on scattering cancellation," Adv. Mater. **24**(44), OP281–OP304 (2012).
24. M. G. Silveirinha, A. Alù, and N. Engheta, "Infrared and optical invisibility cloak with plasmonic implants based on scattering cancellation," Phys. Rev. B **78**(7), 075107 (2008).
25. D. Rainwater, A. Kerkhoff, K. Melin, J. C. Soric, G. Moreno, and A. Alù, "Experimental verification of three-dimensional plasmonic cloaking in free-space," New J. Phys. **14**(1), 013054 (2012).
26. G. Labate, L. Matekovits, A. Monti, F. Bilotti, A. Toscano, L. Vegni, A. Alù, A. Toscano, F. Bilotti, M. Farhat, S. Mühlig, C. Rockstuhl, and F. Lederer, "Scattering cancellation of the magnetic dipole field from macroscopic spheres," Opt. Express **20**(13), 13896–3418 (2012).
27. G. Labate and L. Matekovits, "Invisibility and cloaking structures as weak or strong solutions of Devaney-Wolf theorem," Opt. Express **24**(17), 19245 (2016).
28. A. Monti, F. Bilotti, A. Toscano, and L. Vegni, "Possible implementation of epsilon-near-zero metamaterials working at optical frequencies," Opt. Commun. **285**(16), 3412–3418 (2012).
29. A. Monti, A. Alù, A. Toscano, and F. Bilotti, "Optical scattering cancellation through arrays of plasmonic nanoparticles: A review," Photonics **2**(2), 540–552 (2015).
30. A. Monti, A. Alù, A. Toscano, and F. Bilotti, "Optical invisibility through metasurfaces made of plasmonic nanoparticles," J. Appl. Phys. **117**(12), 123103 (2015).
31. A. Alù and N. Engheta, "Theory and potentials of multi-layered plasmonic covers for multi-frequency cloaking," New J. Phys. **10**(11), 115036 (2008).
32. R. Fleury and A. Alu, "Cloaking and invisibility: A review," Prog. Electromagn. Res. **147**, 171–202 (2014).

Optics EXPRESS

33. M. G. Silveirinha, A. Alù, and N. Engheta, "Cloaking mechanism with antiphase plasmonic satellites," Phys. Rev. B **78**(20), 205109 (2008).
34. A. L. Rodarte, R. J. Pandolfi, S. Ghosh, and L. S. Hirst, "Quantum dot/liquid crystal composite materials: Self-assembly driven by liquid crystal phase transition templating," J. Mater. Chem. C **1**(35), 5527–5532 (2013).
35. M. T. Quint, S. Sarang, D. A. Quint, A. Keshavarz, B. J. Stokes, A. B. Subramaniam, K. C. Huang, A. Gopinathan, L. S. Hirst, and S. Ghosh, "Plasmon-actuated nano-assembled microshells," Sci. Rep. **7**(1), 17788–11 (2017).
36. T. C. Choy, *Effective Medium Theory: Principles and Applications*, 2nd ed (Oxford University Press, Oxford, 2015).
37. R. Mathon and R. L. Johnston, "The approximate solution of elliptic boundary-value problems by fundamental solutions," SIAM J. Numer. Anal. **14**(4), 638–650 (1977).
38. T. Wriedt, A. Doicu, and Y. Eremin, *Acoustic and Electromagnetic Scattering Analysis Using Discrete Sources* (Academic Press, San Diego, 2000).
39. L. L. Foldy, "The multiple scattering of waves. I. General theory of isotropic scattering by randomly distributed scatterers," Phys. Rev. **67**(3-4), 107–119 (1945).
40. M. Lax, "Multiple scattering of waves. II. The effective field in dense systems," Phys. Rev. **85**(4), 621–629 (1952).
41. K. Huang, K. Sølna, and H. Zhao, "Generalized Foldy-Lax formulation," J. Comput. Phys. **229**(12), 4544–4553 (2010).
42. M. Born and E. Wolf, *Principles of Optics*, 7th ed (Cambridge University Press, 1999).
43. A. Ishimaru, *Wave Propagation and Scattering in Random Media* (Wiley-IEEE, 1997).
44. H. C. van de Hulst, *Light Scattering by Small Particles* (Dover, 1981).
45. C. F. Bohren and D. R. Huffman, *Absorption and Scattering of Light by Small Particles* (John Wiley & Sons, 2008).
46. D. I. Yakubovsky, A. V. Arsenin, Y. V. Stebunov, D. Y. Fedyanin, and V. S. Volkov, "Optical constants and structural properties of thin gold films," Opt. Express **25**(21), 25574–25587 (2017).
47. K. M. McPeak, S. V. Jayanti, S. J. Kress, S. Meyer, S. Iotti, A. Rossinelli, and D. J. Norris, "Plasmonic films can easily be better: rules and recipes," ACS Photonics **2**(3), 326–333 (2015).
48. À. González, "Measurement of areas on a sphere using Fibonacci and latitude–longitude lattices," Math. Geosci. **42**(1), 49–64 (2010).
49. A. D. Kim, "*Validating MFS for Mie scattering*" https://github.com/arnolddkim/PlasmonicCloaks (2020).